

1 Thermal failure of a second rotor stage in heavy duty gas turbine

2
3 Daniel Sławiński⁽¹⁾, Paweł Ziółkowski⁽²⁾, Janusz Badur⁽¹⁾

4
5 ⁽¹⁾ Institute of Fluid-Flow Machinery, Polish Academy of Sciences, Fiszerza 14, 80-231, Gdańsk, Poland

6 ⁽²⁾ Gdańsk University of Technology, Faculty of Mechanical Engineering, Department of Energy and
7 Industrial Apparatus, Narutowicza 11/12, 80-233, Gdańsk, Poland

8
9 * daniel.slawinski@imp.gda.pl,

10 11 Abstract

12 The impulse mode of operation and the supply of various types of fuels causes frequent
13 failures even in the heavy duty gas turbines. The paper presents the ravages of second rotor
14 stage failure in a gas turbine. The excessive thermal elongation rise caused by fuel change
15 was indicated as the main cause. We applied nonlinear numerical analysis, preceded by
16 thermodynamic calculations of the turbine and visual inspection of the effects of failure.
17 Simulations were performed on undamaged blade geometry under load resulting from
18 combustion: nominal fuel and the changed fuel. Thermodynamic calculations demonstrated
19 a 70°C increase in temperature using the changed fuel. The blade tip displacements
20 demonstrated the possibility of abrasion. The amount of displacement of the tip of the turbine
21 blade with increasing pressure or increasing rotational speed do not pose as great a threat, as
22 does the increase in the temperature. To maintain long-term and safe operation of a gas
23 turbine, it is necessary to strictly observe the manufacturer's guidelines regarding fuel
24 composition. If during the operation of a gas turbine it is likely that it can be powered by
25 various types of fuels, then the structure should have adequate effort reserves and working
26 tolerances.

27 28 29 1. Introduction

30 The variable mode of operation of power units, dictated by both the significant share of
31 renewable energy sources in the power market, and the requirements set for power turbine
32 sets as to the possibility of supplying them with various types of fuels comprising
33 biocomponents, is a frequent cause for failures. This problem applies to the entire range of
34 power equipment and the most heavily loaded elements within them. Banaszekiewicz [1]
35 indicates this reason as the main source of cracks appearing in the notches of steam turbine
36 rotors. Bryk et al. [2] note issues with 1st degree cracking of stages of steam turbines, caused
37 by the same reason. A gas turbine for stationary energy production has the same operating
38 principle as aircraft turbine sets do. Turbine assemblies, rotating in the result of expansion
39 of compressed exhaust gas, drive the compressor, most often located at the front of the
40 engine, and a generator - in the case of stationary application or a propeller in aviation [3].

1 Due to very high rotational speeds and high exhaust gas temperature, turbine discs and
2 blades are subjected to high loads, which often reach the material strength limits. In order
3 to reduce thermal loads in the blade elements, internal cooling is used to reduce the
4 temperature gradient inside their profile.

5 Gas turbine blades, due to the extremely high loads, are most prone to failure. [4] presents
6 the reasons for the failure of the first stage blade in a 70 MW gas turbine. What was recorded
7 was cracking at various heights around the cooling vents along with degradation of the surface
8 layer of the material due to high temperature. These symptoms resembled those from this
9 failure, given that the blades were made of a similar nickel-base alloy - the Inconel 738LC. It
10 was found that the initiation and propagation of the crack of the coating was driven by the
11 mixed mechanism of fatigue and creep of the material. The degradation of the coating
12 facilitated the initiation of cracks due to thermal fatigue (low cycle fatigue). [5] describes a
13 similar failure mode. In this case it concerned the first stage blade of a smaller, with just 3 MW
14 of power, gas turbine. Following metallurgical examinations, it was found that the main cause
15 of the failure was increased creep of material caused by high temperature operations. Using
16 the FEM analysis and the Larson-Miller parameter (LMP) it determined the loss of service life
17 due to increase in temperature. High-temperature creep in elevated state of stress as the
18 cause of the second stage failure in an aviation turbine was also described in [6].

19 Another type of destruction is one in which the failure is initiated by a foreign body impacting
20 the rotating parts. As a consequence of impact, chipping or localized crack of the blade fin
21 occurs, and the frequency of natural vibrations is altered. As a result of the rupture, the blade
22 becomes unbalanced and thus susceptible to resonance excitations [7]. A slight dent does not
23 necessarily lead to a failure in very short time. It is further proven in [8] describing the high
24 cycle fatigue (HCF) in an aircraft engine compressor. Using the FEM analysis and the Baumel-
25 Seeger method, the number of cycles required for cracking initiation was estimated as a
26 function of excitation amplitude. After reducing the load the number of cycles of the crack
27 initiation increased several times. In [9] the authors describe blade failure in three turbine
28 stages. The investigation demonstrated that damage to the surface coating was caused by
29 strong oxidative corrosion at the leading edge of one of the blades of the first stage. Fatigue
30 cracking was initiated in this pit, spreading deeper into the material during operation. The
31 crack investigated under microscope further proved it. Then the broken elements of the first
32 stage blades caused further damage to the adjacent blades and that of the subsequent stages.
33 The turbine reached 80% of its intended service life, and only several hundreds of hours have
34 passed since its previous overhaul. Operation in a highly corrosive environment and erosion
35 of blades caused by pumping exhaust gases containing solid particles was the cause of the
36 failure described in [10]. The cyclic load and the concentration of stress in surface defects
37 affected the blade fatigue life as a result of increased stress in the main axes and contributed
38 to the reduction of the available life reserve. Stress corrosion cracking of material was
39 described in [11]. The cracking mechanism was manifested in the dovetails for attachment of
40 blades. Various failure mechanisms were considered. The authors were able to eliminate

1 stress concentration in the result of a change in the manufacturing technology changing the
2 transitional radii (i.e. modifications to the groove geometry). The propagation of the crack
3 caused by the corrosive pit in the front part of the profile was examined as the cause of the
4 failure in [12]. The corrosion was the result of compressor's operation in heavy duty
5 environment, and the crack developed according to the mechanism of high cycle fatigue (HCF).

6 Maktuf and Sai describe failure of blade made of Inconel 718, whose primary cause was the
7 high-cycle fatigue (HCF) mechanism initiated in a carbide rich area. The mechanism of brittle
8 cracking developed along the inducing grain boundary brittleness [13]. A material anomaly as
9 a cause of blade failure in a gas turbine was also described in [14]. One of the blades failed,
10 breaking several others in the stage. The blade failed at its shank. Carter described the most
11 common causes of blades failure in gas turbines. While suction of debris is dangerous for the
12 compressor part, the turbine part has its own sources of erosion. These include: unburned
13 coal, deposited as coke around the fuel injection nozzles and detached pieces of ceramic
14 coating on the walls of the combustion chamber. This phenomenon usually occurs when the
15 fuel stream is incorrect or its composition deviates from the nominal one [15]. Metallurgical
16 defects and cavitation pores in the trailing part of the blade profile were the cause of the first
17 stage blade failure described in [16]. Foundry defects found in the trailing part of the profile
18 also caused the failure described in [17].

19 The failure resulting from the development of the high cycle fatigue (HCF) mechanism at the
20 top of fir tree root is described in [18]. It describes the failure of a third stage blade of a 150
21 MW gas turbine. A crack appeared just above the lock at the base of the profile after
22 approximately 22,400 hours of operation. The blade was made of Inconel 738. (The fracture
23 on the turbine blade is located at the top fir tree root.) Fretting fatigue was identified as the
24 underlying cause. [19] describes the destruction of an uncooled blade of a gas turbine. The
25 crack developed from the leading edge towards the trailing edge. Material loss (notch) was in
26 the result of increased stage temperature was identified as the primary cause. What was
27 identified as the secondary cause was the lack of appropriate stage temperature control - i.e.
28 lack of local temperature sensors. Damage occurred at the bandage and halfway up the profile.
29 The place of occurrence of the failure and the effect of high temperature demonstrates great
30 similarity to the damage mechanism described in the present article. Another failure, also
31 caused by overheating of the material, is described in [20]. It describes the destruction of the
32 first stage of a 30 MW gas turbine. Local overheating of the material caused oxidation of the
33 protective top layer made of aluminum (PT-Al). The indentations acted as notches for stress
34 accumulation. Cracks appeared both from the leading edge and the trailing side - similar to
35 the temperature gradient. It was found that blade damage occurred due to the combined
36 effect of surface degradation resulting from overheating, oxidation, hot corrosion and
37 degradation of the heavily oxidized coating. (From these investigations, it is concluded that
38 the failure of gas turbine blade takes place due to the combined effect of surface degradation
39 caused by overheating, oxidation, hot corrosion and degradation of coating heavily oxidized.)
40 Thermal fatigue was the main reason for the destruction of second stage blades in [21]. In



1 addition, high temperature hot corrosion (HTHC) was noted to have an additional effect on
2 the destruction of the surface layer covering the blades. The temperature range in which the
3 damage occurred (850-950 Centigrade) brings these two failures closer together. The blade
4 material was also Inconel. The difference is the long turbine operating time preceding the
5 failure, and the occurrence of rough, porous layer at the surface of the blade at the crack. This
6 layer is characteristic of HTHC.

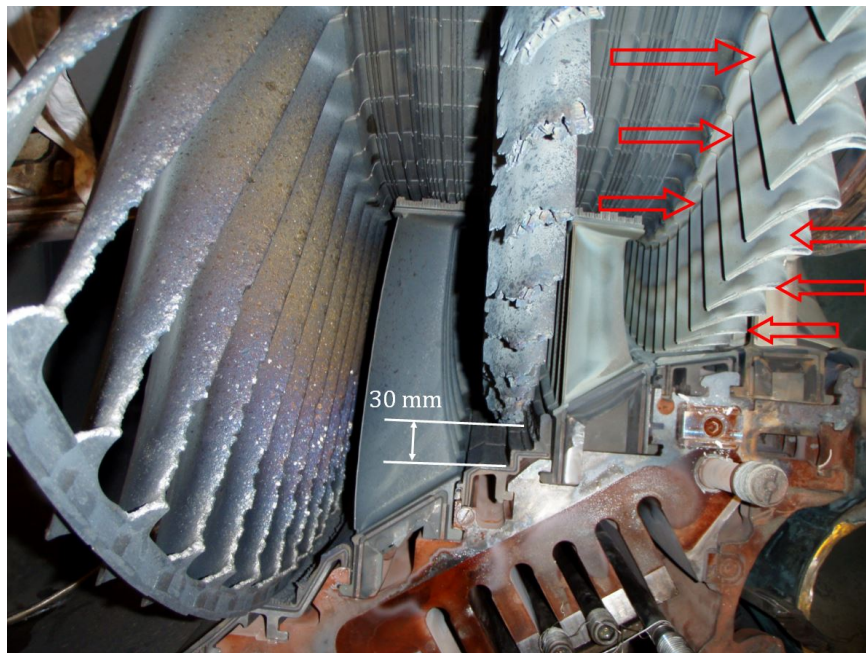
7 Research carried out on a gas turbine blade [22], comparing the effects of a foreign body
8 impact to high temperature operation, have undeniably demonstrated the more destructive
9 effect of high temperature. The scope of the study covered temperatures from 20 C to 900 C.
10 Microscopic evaluation revealed the mechanism of transgranular cleavage. Traces of material
11 overheating [23] and mechanisms of thermal fatigue were noticed in the leading part of the
12 profile. Operation at a temperature that is higher than the nominal one led to the destruction
13 of the top protective coating. The location of failure was also at the foot of blade, which makes
14 it similar to that described in the present work. [24] describes the effect of exhaust gases and
15 temperature on the degradation of heat-resistant coatings in gas turbines. It has been found
16 that during the exploitation the quality of coatings decreases non-linearly, which results in
17 deterioration of their protective properties.

18 The purpose of my work is to find the causes of failure of the second stage blade in a high
19 power gas turbine operating in one of the specialized power plants. Some of the symptoms
20 and destruction mechanisms discussed here interact with those noted on the object. Some,
21 however, differ significantly, which makes the failure intriguing, and yet difficult to clearly
22 classify and solve. The failure occurred in the absence of anomalies related to the increased
23 amplitude of vibrations, and the staff did not hear noises, which are symptomatic of the
24 impact nature of the failure, coming from the casing. There was more than sufficient time left
25 in the planned turbine maintenance schedule. The only deviation was the change to a fuel
26 with the same calorific value but with a different density. The fuel composition was identical,
27 which was further proved by relevant certificates. Additional features not found in the subject
28 literature were: the unusual location of blade failure - the tip, under the bandage and the long
29 duration of the failure - a dozen or so minutes. It should be mentioned that the entire rotor
30 demonstrated the same even form of "melting" of the upper layers, and no blades were torn
31 off at the base, as suggested by the literature. There are also no porous surfaces characteristic
32 of high temperature corrosion (HTHC). In the present article we pay attention to the analysis
33 of the mechanisms of destruction resulting from a structural error (failure to adjust the size
34 of the gap above the bandage to the thermal expansion of material resulting from use of
35 alternative fuels) but also to thermal fatigue (low cycle fatigue).

36 2. Visual examination of failed blade

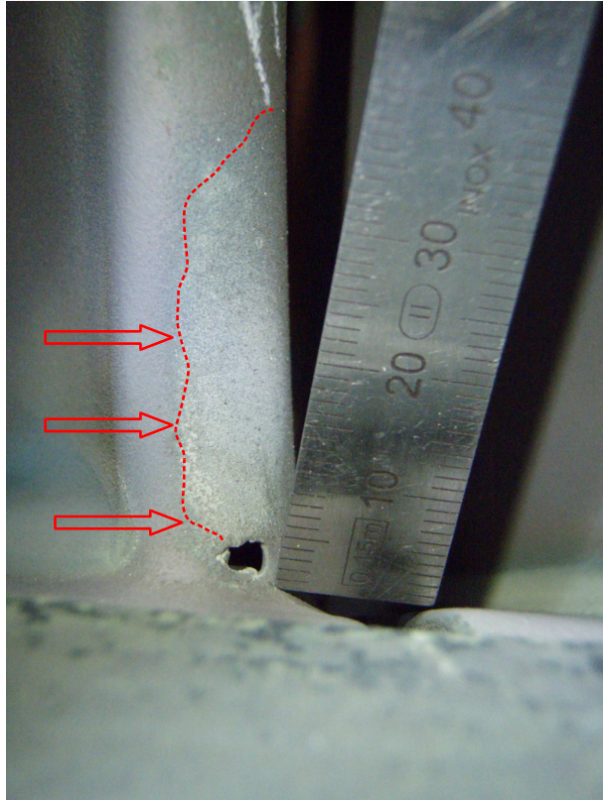
37 The gas turbine blade was broken in the upper part of the blade, near the bandage. The even
38 melting of all blades of the rotor stage and the jagged nature of the damage proves that we
39 are dealing with failure resulting from the presence of a large heat source. This source was,

1 most likely, (Fig. 1) the friction of the rotating blade bandages against the seals separating the
2 body case. The specific stepped shape of this seal, which has no equivalent in subject
3 literature, is also not without significance here.



4
5 Figure 1 View of the 2nd stage following the failure with a characteristic even melting
6 of the upper parts of the blades.

7 The melting occurred evenly, stopping at a distance of 30 mm from the internal walls of the
8 body case. An additional argument in favour of thermal damage to the blades are tarnish
9 indicated by arrows, clearly visible on the first stage of the turbine. These stains are the result
10 of high temperatures, and their formation is primary in its nature, resulting from too high a
11 temperature of the flowing exhaust gas. In an interview with the power plant operator, we
12 determined that the failure was preceded by a change in the fuel supplied to the turbine.

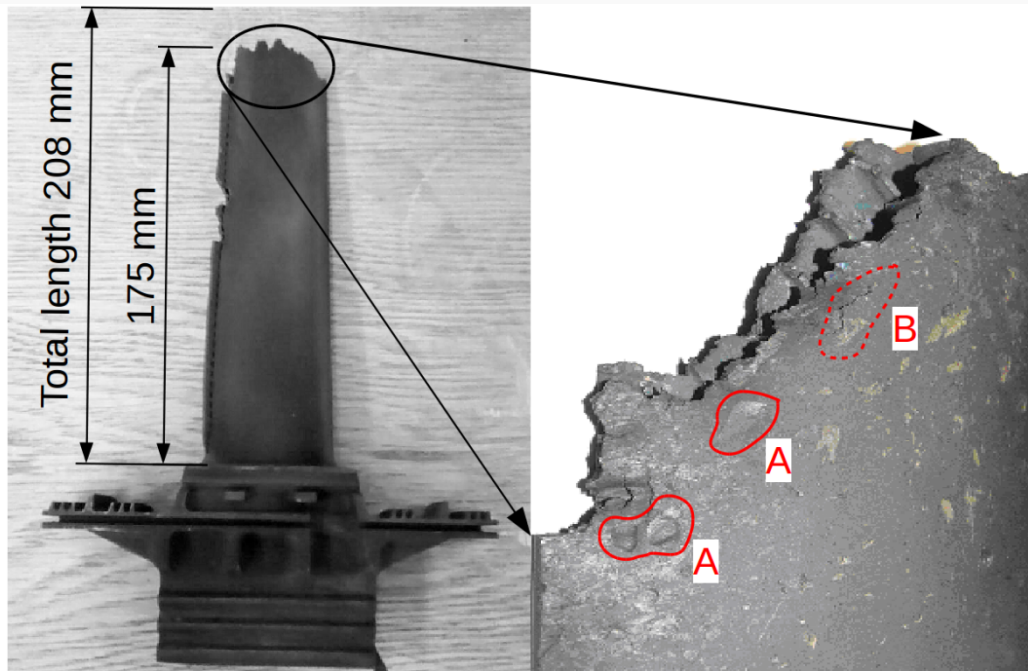


1
2 Figure 2 Damage to the blade profile at the base and characteristic discoloration
3 resulting from the effects of high temperature.

4 Another damage of this type observed after a failure was the discoloration located (Fig.2) in
5 the lower part of the blade in the place of the profile face. This discoloration was discovered
6 on the blade of the 2nd rotor stage and its dimensions are similar to those found on the 1st
7 rotor stage, and marked in the previous figure. A small hole with a diameter of 5 mm was
8 found at the base of the profile. Its creation was probably the result of high temperatures and
9 mechanical loads.

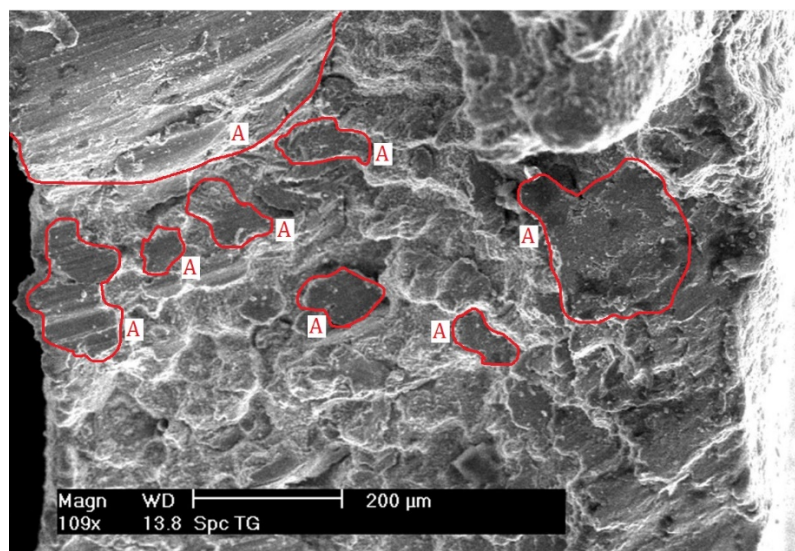
10 This section contains images of the blade after failure captured by scanning microscopy
11 (SEM). Visual inspection confirmed that during the failure the rotor blades were in good
12 condition and observations under the microscope ruled out micro-cracks on the blade
13 surface as well as corrosion or high temperature creep effects (Fig.3). Visible dents or cracks
14 of the surface layer of the blade are the consequence of failure, and occurred during the said
15 failure in the result of impact of pieces of hot and detached steel on the remaining blades in
16 the said stage. They did not have the nature of the primary cause of the failure, but were its
17 consequence.

18
19



1
2 Figure 3 Macroscopic image of the damaged blade with the following references: A)
3 dents and surface layer damage, and B) cracks formed during the development of failure.

4 Based on the macroscopic image of the damaged location and its image at low magnifications,
5 it can be assumed that the observed fracture does not belong to the group of trans-crystalline
6 cleavage. SEM images shown in Fig.4 at the highest magnifications show the occurrence of
7 facets that link through plastic deformation [25], which allows us to classify the fracture as the
8 quasi-cleavage type.



9
10
11 Figure 4 View of the fracture magnified 109, (A) describes the places of cleavage,
12 which gives the whole section the character of quasi-cleavage.

13 The change in fuel composition led to an increase in exhaust gas temperature in successive
14 turbine stages. Strong overheating of the material around the upper bandage in the result of

the bandage abrading against the corps, led to cracking due to a decrease in material properties and the initiation of the low cycle fatigue (LCF) process. The blade loading forces - not including friction effects - were standard ones, resulting from the rotational speed and aerodynamic forces caused by the flow of exhaust gases.

3. Finite element model of the blade

3.1. Theoretical aspects of blade failure

3.1.1. Equation of momentum and energy balance

The equation for rotating blade motion and immovable sealing was described by the same thermal-FSI mathematical model consisting of: equation of momentum and energy balance:

$$\rho \partial_t \mathbf{v} = \text{div} \boldsymbol{\sigma} + \rho \mathbf{b} \quad (1)$$

$$\rho \partial_t (c_p T) = \text{div} \mathbf{q} + \boldsymbol{\sigma} \cdot \dot{\boldsymbol{\varepsilon}} + \rho \mathbf{b} \mathbf{v} \quad (2)$$

where: \mathbf{v} is the overall velocity vector (m/s), \mathbf{b} are mass forces ($\mathbf{b} = -g \mathbf{e}_x$, $g = 9,81$ (m/s²), T , c_p are temperature (K) and specific heat capacity at constant pressure (J/kg K).

Constitutive equation of thermo-elastic stress tensor and total strain tensor defined by formula:

$$\boldsymbol{\sigma} = 2\mu \boldsymbol{\varepsilon} + \lambda (\text{tr} \boldsymbol{\varepsilon}) \mathbf{I} + \beta (T - T_0) \mathbf{I} \quad (3)$$

$$\boldsymbol{\varepsilon} = \frac{1}{2} (\text{grad} \mathbf{u} + \text{grad}^T \mathbf{u}) \quad (4)$$

Where: μ, λ is Lama'e constants, \mathbf{I} is Gibbs unite tensor ($\mathbf{I} = \delta_{ij} \mathbf{e}_i \otimes \mathbf{e}_j$, \otimes is dyadic multiplier), \mathbf{u} is tensor of deformation and T_0, β are referential temperature, and constant of thermal strain ($\beta = E\alpha$) respectively, E are Young module (MPa), α are constant of thermal strain (1/K).

3.1.2. Estimation of heat flux generated during friction of the bandage against the gas turbine seal

The source of heat flux generated as a result of friction between the bandage and the seal was described by the formula:

$$\mathbf{q} = \boldsymbol{\sigma} \mathbf{v} |^A = \boldsymbol{\sigma} (\omega r \mathbf{e}_\varphi) |^A \quad (5)$$



1
2 where: ω , r is angular speed (1/s) and radial dimension (m) respectively, \mathbf{e}_φ are a versor and
3 A is the contact area of the blade solid with the seal medium.

4
5 The total amount of energy generated as a result of friction was recorded in the formula

$$6 \quad E = \int_{\tau_0}^{\tau} \iint_A \mathbf{q} \cdot \mathbf{n} dA = n \cdot \boldsymbol{\sigma}(\omega r \mathbf{e}_\varphi) A (\tau - \tau_0) \quad (6)$$

7 The value of the γ coefficient separating the heat flux into the part flowing into the bandage
8 of the blade and the seals was recorded [26].

$$9 \quad \gamma = \frac{\kappa^b \sqrt{\kappa^w}}{\kappa^b \sqrt{\kappa^w} + \kappa^s \sqrt{\kappa^b}} \quad (7)$$

10 where: κ^b , κ^s are respectively heat conduction coefficients at the bandage and the seals (W/m
11 K).

12
13 After calculating the γ coefficient, the heat flux splits into parts affecting the blades and seals:

$$14 \quad \mathbf{q}^b = \gamma \mathbf{q}, \quad \mathbf{q}^s = (1 - \gamma) \mathbf{q} \quad (8)$$

15 where: b , s are subscripts at bandage and seal respectively.

16 17 **3.1.3. A Cycle-rapture model based on Manson's criteria**

18
19 The main causes causing thermal fatigue are mechanical deformations, resulting from
20 blocking the movement of connections. These connections prevent free movement of
21 machine parts in the result of cyclical temperature changes [27]. Thermal fatigue is
22 considered as a process in limited number of cycles. According to Jakowluk [28], this process
23 is characterized by crack formation mechanisms similar to those of creep and mechanical
24 fatigue. Therefore, it is treated as a accumulation of two processes: the process of cyclic
25 deformation (primarily plastic) and creep [29].

26
27 The criterion given by Manson proves correct for the cases of thermal fatigue

$$28 \quad \Delta \varepsilon = \varepsilon_f^{0.6} N_f^{-0.6} + 3.5 \frac{R_m}{E} N_f^{-0.12} \quad (9)$$

29 Where: ε_f corresponds to deformations during a static tensile test, N_f is the number of cycles
30 required to destroy the material, and R_m , E are, respectively, the tensile strength during the
31 static test and the Young's modulus. Material data depends on temperature.

32 33 34 **3.1.3 A Creep-rapture model based on regression analysis technique**



1
2 In order to estimate the time required for destruction of material in the result of creep as a
3 function of stress and temperature, we applied formulas developed for Alloy 718 type of alloys
4 at Oak Ridge National Laboratory (ORNL), Idaho National Engineering Laboratory and General
5 Electric (GE) consortium. These formulas were developed on experimental results and are
6 correct for temperatures starting from 760 °C and upwards.

7
8 The first technique is the lot-centered regression analysis technique created by formula:

$$9 \quad \log t_r = C_h - 193.662 \log \sigma + 88.117 (\log \sigma)^2 - 12.807 (\log \sigma)^3 - 0.01052 T \log \sigma \quad (10)$$

10 where the base for all logarithms is 10, and t_r is rapture life (hr), σ is stress (MPa), and T is
11 temperature (K).

12
13 The second technique is the Minimum Commitment Method (MCM) using Manson's two
14 constant, written by formula [29]:

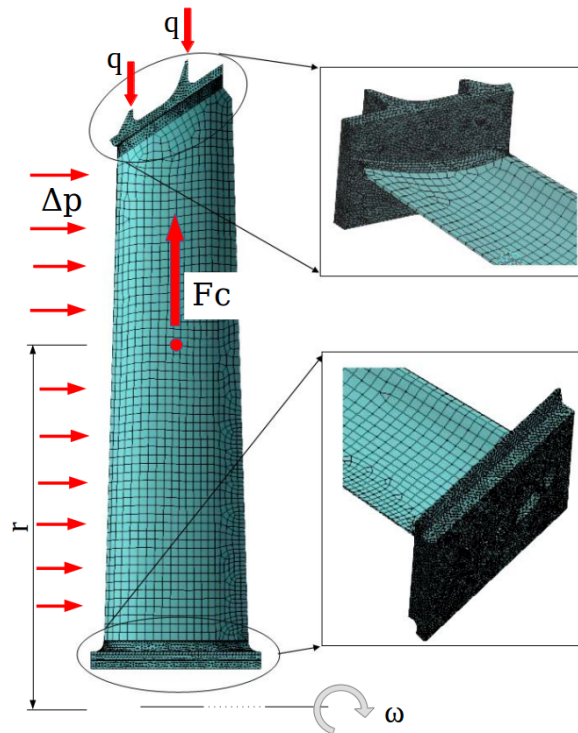
$$15 \quad \log t_r + \left[R_1(T - T_{middle}) + R_2\left(\frac{1}{T} - \frac{1}{T_{middle}}\right) \right] = A + B \log \sigma + D \sigma + E \sigma^2 \quad (11)$$

16 where the constants R_1, R_2, D and E were determined to be $2.14547 \cdot 10^{-2}$, -5622.76 , $-$
17 $2.71294 \cdot 10^{-3}$ and $-2.96015 \cdot 10^{-6}$, respectively. The constants A and B are 9 and -1.6
18 respectively.

19
20

21 **3.2. Grid and boundary conditions**

22 To perform the numerical simulation, we executed a 3D blade model for the blade prior to the
23 failure. In the model (Fig.5) the exact shape of the upper bandage and a small portion of the
24 blade foot are reproduced to determine the causes of the crack at the base of the profile. The
25 geometry of internal flow channels for cooling the blade was also mapped.



1
2 Figure 5 Model of a blade before destruction after its discretization with a mesh of
3 finite elements and marked boundary conditions.

4 The numerical model and calculation grid were executed with use of Design Modeler, which
5 is a module of the Ansys calculation suite. The computational grid had 410,000 20-nodal finite
6 elements.

7 Two simulations were carried out during the study. The first consisted in mapping the
8 temperature and stress distribution using design conditions for the turbine stage subject to
9 our investigation - the results were adopted as reference. The second simulation consisted in
10 mapping the above mentioned fields for the case with increased gas temperature and
11 presence of rubbing of the upper bandage against the body of the gas turbine. The results of
12 this simulation were compared with the images of the blade obtained as a result of visual
13 inspection after the failure. The comparison allowed to determine the degree of accuracy of
14 failure mapping in the numerical simulation.

15 The blade was attached from below. The load was surface forces resulting from the
16 aerodynamics of gas flow in the said stage and centrifugal forces, caused by rotor speed, blade
17 mass, as well as the distance of its centre of gravity from the axis of rotation. The heat flux
18 generated as a result of abrading the seals formed the additional boundary condition. The
19 predefined temperature field was similar to the nominal work of turbine stage.

20
21 **4. Results of numerical simulation**



4.1. Thermodynamic parameters in 2nd stage of the gas turbine

In order to determine the operating parameters before and after the second turbine stage, the COM-GAS numerical code was used. This code is used for calculating thermodynamic cycles, and was created and is still applied in the Department of Energy Conversion of the IMP PAN in Gdańsk [30]. The analysis was carried out for two types of fuel. The first one was natural gas with parameters for which the turbine was designed. The second was mixed gas, which was supplied interchangeably to the power plant from the nearby Oil Mine. Fuel change, as already mentioned in the previous item, shortly preceded the occurrence of failure.

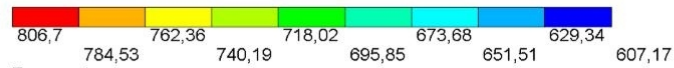
The data contained in the reports demonstrate that the differences in heating values of natural gas and mixed gas were significant. These values were estimated at 19.208 MJ/kg for natural gas and 20.640 MJ/kg for mixed gas. It should also be emphasized that the calorific values for both gases related to a unit of volume were similar and amounted to 20.57 MJ/m³ and 20.32 MJ/m³. These values were decisive in allowing mixed gas as a replacement fuel [31].

Calculations of the thermodynamic cycle carried out with the COM-GAS code demonstrated that, following the change of fuel [32], the temperature at the outlet of second stage increased from 815 to 850 °C. The pressure difference at stage inlet and outlet remained unvaried and amounted to 0.5 MPa. The blade cooling flow was 2.9 kg/s for the whole stage, which for 88 blades in question corresponded to - 0.0329 kg/s per 1 turbine blade. The cooling air temperature was taken after 6th stage of compressor and amounted invariably to 235 °C.

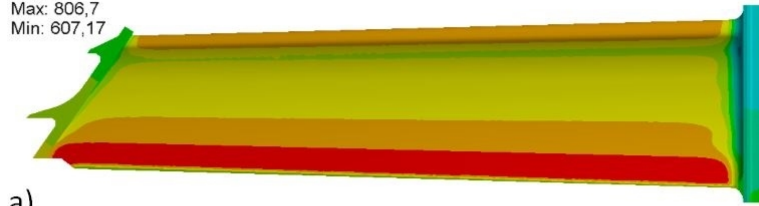
4.2 Results of the finite element calculation

Numerical simulation was performed using the Ansys program. The analysis included steady state calculations in which the heating-up effects of the blade and turbine were omitted. Comparison of temperature fields for supplying the turbine stage with nominal gas and mixed gas is shown in Fig.6. For gas supply with nominal parameters, the temperature field does not exceed 811 °C. The location of temperature extremity is at the trailing edge of the blade and on the front of the profile. In the bandage area (Fig.6.a) the temperatures did not exceed 740 °C. In the case of gas with changed composition, the temperatures increased by about 50 °C for the trailing edge and profile face, and by 30°C in the bandage. The fields did not vary significantly in shape. It should be noted here that the areas with the highest temperatures correspond to discoloration that was detected during visual inspection of the turbine stage (see Figs. 1 and 2).

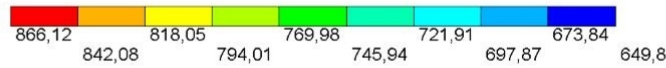




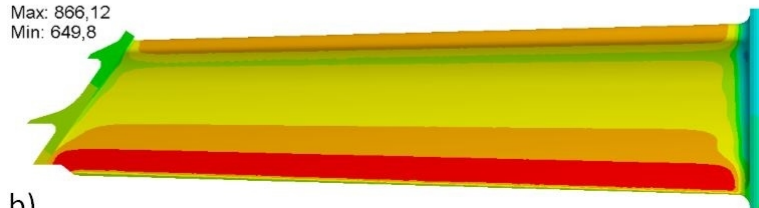
Temperature
 Type: Temperature
 Unit: °C
 Custom
 Max: 806,7
 Min: 607,17



a)



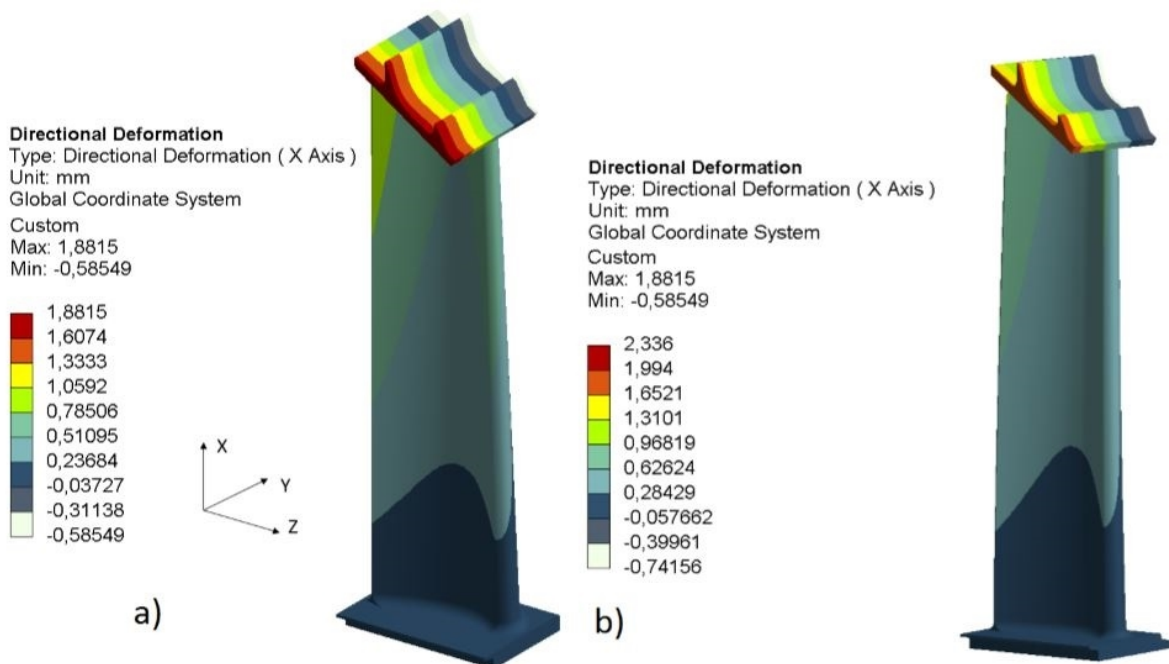
Temperature
 Type: Temperature
 Unit: °C
 Custom
 Max: 866,12
 Min: 649,8



b)

1
 2 Figure 6 Temperature field, as numerically estimated a) for nominal gas parameters;
 3 and b) after change.

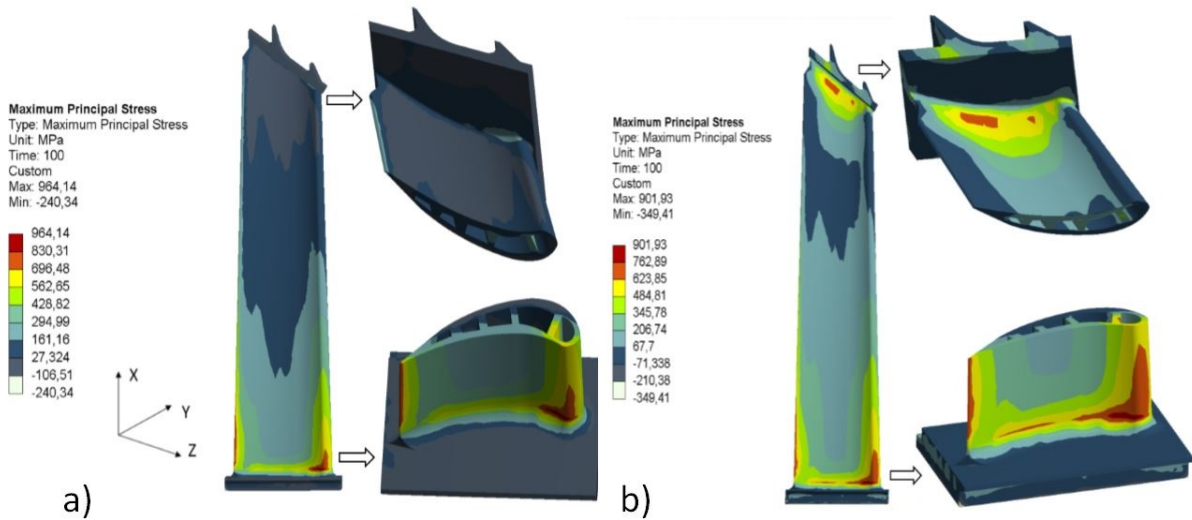
4 Displacement fields for both cases are shown in Fig.7. Not only did the displacement values
 5 change, but also their area, which resulted in a change in the blade deflection mode. The
 6 value of the maximum radial displacement when using the replacement fuel increased from
 7 1.14 to 2.13 mm. The resulting displacement field generated stresses inside the blade
 8 material.



9

1 Figure 7 Blades displacement in radial direction for a) nominal gas parameters; and b)
 2 after change of fuel.

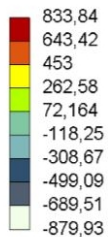
3 The study analyzes the components of a stress tensor perpendicular to the direction of the
 4 scrap metal. These stresses have the largest contribution to the initiation and development of
 5 cracks in the blade shells [25]. These will be: the maximum principal stresses S_1 and normal
 6 stresses σ_{xx} acting parallel to the direction of load.



7
 8 Figure 8 Main stress field read in radial direction for a) nominal gas; and b)
 9 after fuel change.

10 The maximum principal stresses were read during nominal operation and after the fuel
 11 change. For the nominal case (Fig.8.a) maximum stress is concentrated around the base of the
 12 blade, which is consistent with the theory of design turbine blades. In the event of a fuel
 13 change we observed areas of stress concentration in the area of the base and bandage.
 14 Stresses reach up to 126 MPa, and in the place of the greatest strain at the base, they increase
 15 to 395 MPa.

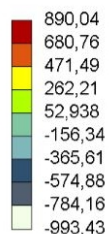
Normal Stress
 Type: Normal Stress (X Axis)
 Unit: MPa
 Global Coordinate System
 Time: 100
 Custom
 Max: 833,84
 Min: -879,93



a)



Normal Stress
 Type: Normal Stress (X Axis)
 Unit: MPa
 Global Coordinate System
 Time: 100
 Custom
 Max: 890,04
 Min: -993,43



b)

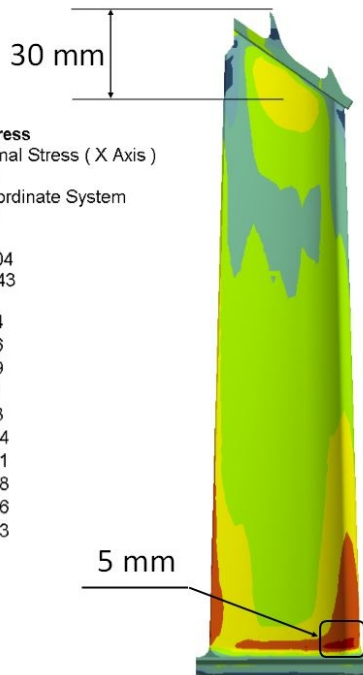


Figure 9 Normal stress field read in radial direction for a) nominal gas; and b) after fuel change.

For more details, the differences in stress values are shown in Fig. 9. The contours of maximum stress are located around the base of the profile, focusing on the front part and on the trailing edge. In the bandage area, stress of 116 MPa was read. In the event of change of fuel, these stresses increased their value to some 450 MPa. Another observation is the small stress concentration area near the profile face at its base. After changing the fuel, the value of stresses read there increased from 480 to 840 MPa. Such high stresses did not exceed a circle with a diameter of 5 mm. The distance between the centre of the stress field around the bandage and the top of the highest seal was 30 mm. This value is identical to that measured during the visual inspection of the failure and previously marked in Fig.1. Also the field of stress concentration at the base of the turbine blade in area coincides with the hole shown in Fig.2.

4.3. Estimating blade service life

After examining the blade under a microscope and with the results of numerical simulations at hand, also knowing the flow conditions and temperatures prevailing in the degree, we performed an estimation of time to failure. The graphs presented are based on theoretical models discussed in previous items.

As the first method we applied the Manon's criteria. The results of these calculations are presented in Fig. 10. The presented values were read from the most strenuous area located at the bandage.



1 Two curves were drafted, presenting the relationship of the amount of deformation to the
 2 number of cycles required to destroy the material. The first (upper) curve presents the
 3 relationships for the nominal operating conditions of the stage powered by reference fuel.
 4 The calculated point is located at the bottom of the graph, indicating some 50 000 cycles to
 5 failure. This value is close to the design value, which for heavy duty stages equals 100 000
 6 cycles. The magnitude of deformations also falls below the critical line.
 7 After changing the fuel and increasing the stage temperature, the read size of deformations
 8 increases drastically, adopting the location of the critical curve drafted for the changed fuel.
 9 Now the number of cycles to failure reads about 20.

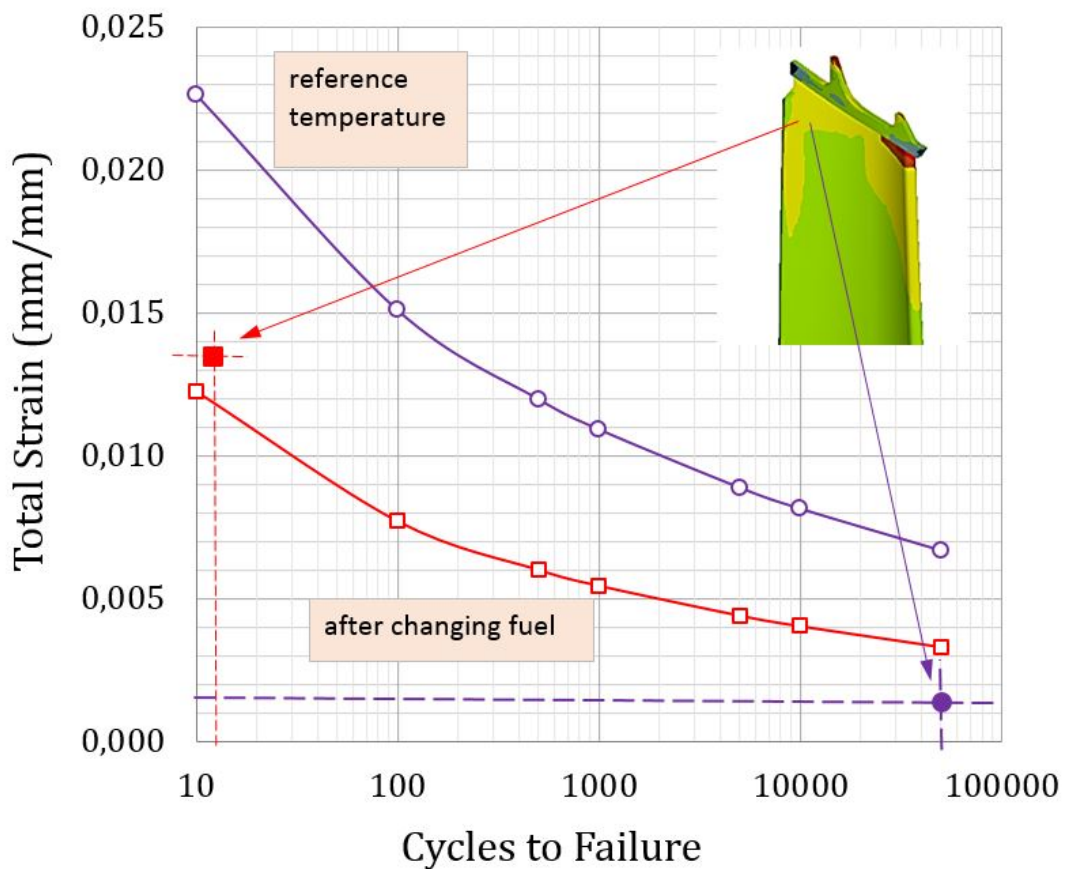


Fig. 10 Estimated number of cycles to failure by using Manson's criteria

10
11
12
13
14
15
16
17
18
19
20

A similar relationship was observed when plotting the relation of service life to the magnitude of stress generated in the blade. The results are presented in Fig.11. Stresses generated in the blade during nominal operation are below the critical line indicating an estimated service life of approximately 10 000 hr. The resulting value is also acceptable in terms of design criteria. After changing the fuel, the increasing stress caused the crossing of critical line, thus determining the value of service life at just 10 hr. This change in available service life is drastic and should not be left unnoticed.

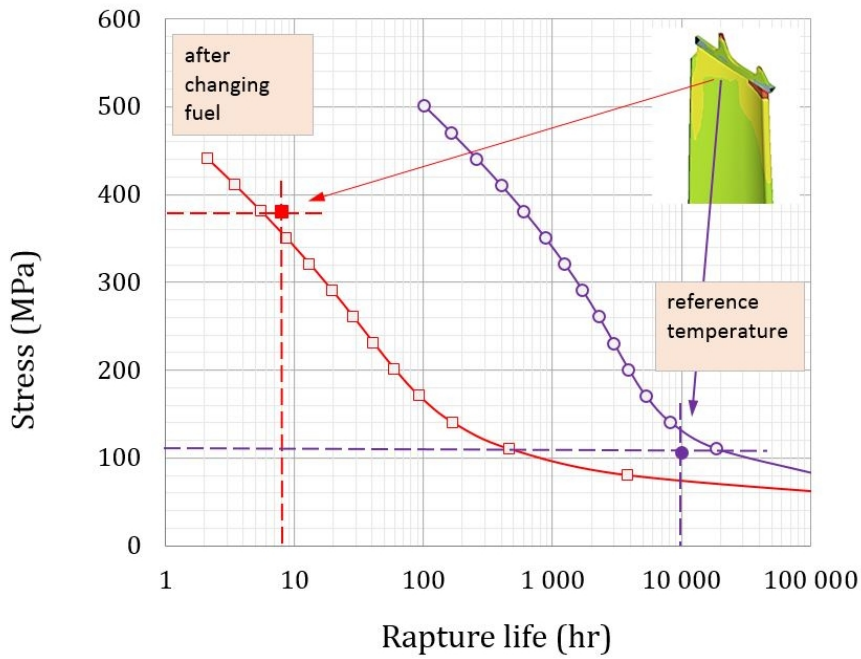


Fig. 11 Estimated time to failure using the first technique of data description.

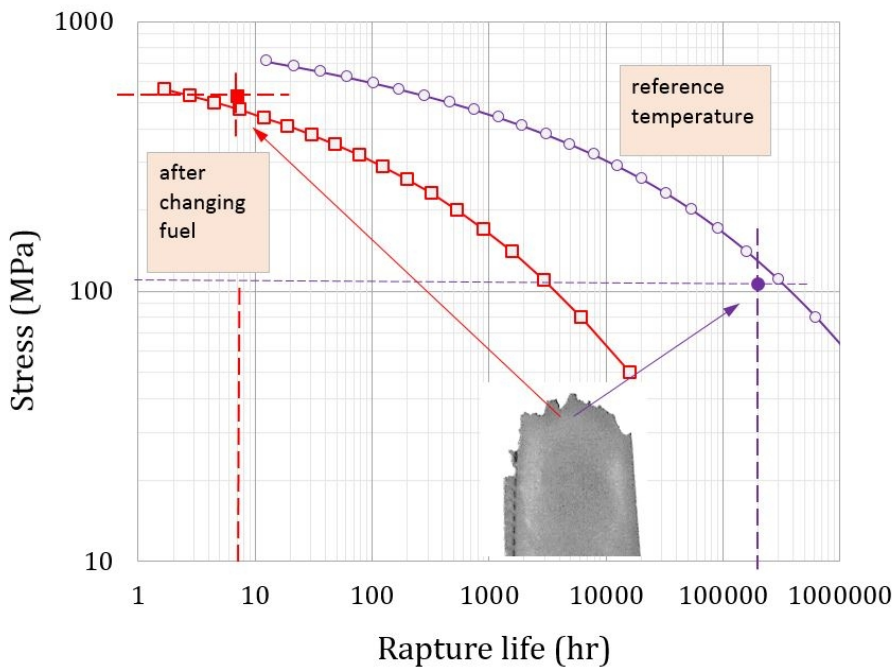


Fig. 12 Estimated time to failure using the second technique of data description.

The results presented in Fig. 12, confirm the existing rule. Stresses read in the blade material in the FEM analysis indicated the possibility of seamless blade operation of up to 200 000 hr. Changing the fuel, and thus the working conditions of the stage and stress of materials reduced the permissible operating time to 8 hr. These results are consistent with previous observations.



5. Conclusions

The paper presents an analysis of the destruction of a 2nd stage blade in a heavy duty gas turbine. From the beginning it was obvious and unambiguous that increasing the temperature to a degree above design values would lead to its overstressing or complete destruction. Visual analysis following the failure and numerical simulations demonstrated that the likely consequence of the temperature rise was that the blade abraded against the seals, and a further increase of temperature in the bandage area.

Simulations of the thermodynamic cycle demonstrated that when changing the type of fuel from natural gas to mixed gas, while maintaining a similar volumetric calorific value of fuel, and failing to observe the gas density, it is possible to increase the temperature of the exhaust gas in the combustion chamber. This consequently causes a simultaneous increase in the temperature of the blade material and an increase in its elongation causing abrasion of the bandage of the rotor blades against the seal and turbine body.

The results of numerical simulation also demonstrated that the change in the amount of displacement resulting from spinning and aerodynamic forces is small compared to deformations caused by high temperature. As long as the design temperature of the turbine stage is met, even significant fluctuations in pressure or rotating speed should not compromise the service life of the stage.

The analyses estimating the number of cycles to failure and the safe service life leave no space for doubt. Both the blade and the entire stage were not designed to operate in such a temperature. The use of changed fuel, by causing an increase in stage temperature and blade stresses, dramatically reduced the service life of the blade, from its initial design value, to just several hours.

This situation can be blamed on higher amount of head leading to a low cycle failure (LCF) and high susceptibility of the material to change of its properties within the considered temperature ranges. Errors in design, which should protect against this type of incident, allowing the turbine to be supplied with various types of fuels, are also not devoid of significance.

6. Recommendations

1. Strict adherence to the manufacturer's recommendations on how to drive the machine, its operating parameters, the composition of the fuel used and operating fluids.
2. The use of replacement fuels whose properties have not been taken into account in the design process of the heavy duty gas turbine, even for a short period of time, can



1 significantly reduce the service life of its sensitive components or trigger a large scale
2 failure.

3 3. It is recommended that sensitive machine components susceptible to frequent and
4 costly repairs are equipped with additional systems for monitoring their effort and
5 durability during operation.

6 4. If, during the operation of a heavy gas turbine, it is likely that it can be fuelled with
7 various types of fuels, the design should contain corrected strain reserves and working
8 tolerances.

10 References

11 [1] Banaszkiwicz M, Numerical investigations of crack initiation in impulse steam turbine
12 rotors subject to thermo-mechanical fatigue, *Appl. Therm. Eng.* 138 (2018) 761-773.

13 [2] Badur J, Bryk M, Accelerated start-up of the steam turbine by means of controlled
14 cooling steam injection, *Energy* 173 (2019) 1242-1255.

15 [3] Witek L, Wierzbińska M, Poznańska A, Fracture analysis of compressor blade of a
16 helicopter engine, *Eng Fail Anal* 16 (2009) 1616-1622.

17 [4] Mazur Z, Luna-Ramirez A, Juarez-Islas J.A, Failure analysis of a gas turbine blade made of
18 Inconel 738LC alloy, *Eng Fail Anal* 12 (2005) 474-486.

19 [5] Kargarnejad S, Djavanroodi F, Failure assessment of Nimonic 80A gas turbine blade, *Eng
20 Fail Anal* 26 (2012) 211-219.

21 [6] Salam I, Taugir A, Creep-fatigue failure of an aero engine turbine blades, *Eng Fail Anal* 9
22 (2002) 335-347.

23 [7] Witek L, Bednarz A, Stachowiak F, Fatigue analysis of compressor blade with simulated
24 foreign object damage, *Eng Fail Anal* 58 (2015) 229-237.

25 [8] Witek L, Numerical stress and crack initiation analysis of the compressor blades after
26 foreign object damage subjected to high-cycle fatigue, *Eng Fail Anal* 18 (2011) 2111-2125.

27 [9] Kumari S, Satyanarayana D.V.V, Failure analysis of gas turbine rotor blades, *Eng Fail Anal*
28 45 (2014) 234-244.

29 [10] Kazempour-Liacy et al, Corrosion and failure analysis of a forced draft fan blade, *Eng Fail
30 Anal* 18 (2011) 1193-1202.



- 1 [11] Banaszekiewicz M, Rehmus-Forc A, Stress corrosion cracking of 60 MW steam turbine
2 rotor, Eng Fail Anal 51 (2015) 55-68.
- 3 [12] Mokaberi A, Derakhshandeh-Haghighi R, Fatigue fracture analysis of gas turbine
4 compressor blades, Eng Fail Anal 58 (2015) 1-7.
- 5 [13] Maktouf W, Sai K, Multiaxial high-cycle fatigue criteria and life prediction: Application to
6 gas turbine blade, Int J Fatigue 92 (2016) 25-35.
- 7 [14] Maktouf W, Sai K, An investigation of premature fatigue failures of gas turbine, Eng Fail
8 Anal 47 (2015) 89-101.
- 9 [15] Carter T.J, Common failures in gas turbine blades, Eng Fail Anal 12 (2005) 237-247.
- 10 [16] Qu S, Fu C.M et al, Failure analysis of the 1st stage blades in gas turbine engine, Eng Fail
11 Anal 32 (2013) 292-33.
- 12 [17] Kim H, Study of the fracture of the 1st stage blade in an aircraft gas turbine, Eng Fail
13 Anal 16 (2009) 2318-2324.
- 14 [18] Barella S. et al, Failure analysis of third stage gas turbine blade, Eng Fail Anal 18 (2011)
15 386-393.
- 16 [19] Mishra R.K. et al, Failure of an un-cooled turbine blade in an aero gas turbine engine,
17 Eng Fail Anal 79 (2017) 836-844.
- 18 [20] Rani S, Agrawal A.K, Failure analysis of first stage INC738 gas turbine blade tip cracking
19 in thermal power plant, Case Stud Eng Fail Anal 8 (2017) 1-10.
- 20 [21] Chaharlang R, Hajjari E, Baghal S.M, Premature damage of the second stage nozzle
21 guide vanes of a gas turbine made of Inconel 738LC, Eng Fail Anal 105 (2019) 803-816.
- 22 [22] Golezani A.S, Bageri M, Samadi R, Microstructural change and impact toughness
23 property of Inconel 738LC after 12years of service, Eng Fail Anal 99 (2016) 624-629.
- 24 [23] Guo X, Zheng W, Evaluation of microstructural degradation in a failed gas turbine blade
25 due to overheating, Eng Fail Anal 103 (2019) 308-318.
- 26 [24] Bogdan M, Błachnio J, Assessment of usability of the exploded gas turbine blade heat-
27 resistant coatings, Eng Fail Anal 105 (2019) 337-346.



- 1 [25] Kocańda S. Zmęczeniowe niszczenie metali [Fatigue failure of steel], Warszawa; WNT
2 1972 [in polish].
- 3 [26] Adamowicz A, Grześ P, Influence of convective cooling on a disc brake temperature
4 distribution during repetitive braking, Appl. Therm. Eng. 31 (2011), 2177-2185.
- 5 [27] Jakowluk A, Procesy pełzania i zmęczenia w materiałach [Process of creep and fatigue in
6 materials], Warszawa: WNT, 1993 [in polish].
- 7 [28] Hales R, Fatigue testing methods at elevated temperatures. Fatigue at high
8 temperatures, Appl. Sci. Publ., London-New York 1983, 63-96.
- 9 [29] Manson S.S, Muralidharan U, Analysis of creep rapture data for five multi-heat Alloys by
10 the Minimum Commitment Method using double heat term centering, Progress in Analysis
11 of fatigue and Stress rapture, MPC-23, ASME, 1984, 1-46.
- 12 [30] Ziółkowski P, Badur J, Ziółkowski P.J, An energetic analysis of a gas turbine with
13 regenerative heating using turbine extraction at intermediate pressure - Brayton cycle
14 advanced according to Szewalski's idea, Energy 185 (2019) 763-786.
- 15 [31] Ziółkowski P, Lemański M, Badur J, Power augmentation of PGE Gorzow's gas turbine by
16 steam injection-thermodynamic overview, Rynek Energii 98 (2012) 161-168.
- 17 [32] Ziółkowski P, Kowalczyk T, Lemański M, On energy, exergy, and environmental aspects
18 of a combined gas-steam cycle for heat and power generation undergoing a process of
19 retrofitting by steam injection, Energy Convers Manage 192 (2019) 374-384.

20

